South African Journal of Chemical Engineering 42 (2022) 162–175

Contents lists available at ScienceDirect

South African Journal of Chemical Engineering

journal homepage: www.elsevier.com/locate/sajce

Acid-activated *Hibiscus sabdariffa* seed pods biochar for the adsorption of Chloroquine phosphate: Prediction of adsorption efficiency via machine learning approach.

Deborah Temitope Bankole [a], Abimbola Peter Oluyori [a], Adejumoke Abosede Inyinbor [a,b,*]

[a] Department of Physical Sciences, Landmark University, P.M.B 1001, Omu Aran, Nigeria
[b] Clean water and Sanitation Sustainable Development Goal, Landmark University, P.M.B 1001, Omu Aran, Nigeria

ARTICLE INFO

Keywords:
Characterization
Artificial Neural Network
Adsorption
Pharmaceuticals

ABSTRACT

A constant increase in the release of pollutants into the environment poses a threat as this practice continually degrades water quality. One of the proffered solutions is the adsorption of pollutants onto adsorbents. The present study emphasized the performance of *Hibiscus sabdariffa* seed pods (HSP1) for removing Chloroquine phosphate (CQ) from aqueous media via adsorption. A machine learning tool (Artificial Neural Network, ANN) was used to predict the efficiency of CQ removal onto the prepared biochar. Different operational parameters were investigated for their influence and impact on CQ adsorption. HSP1 was also characterized using different physicochemical and spectrophotometric techniques. HSP1 remarkably displayed an outstanding performance for the elimination of CQ with a q_{max} of 161.29 mg/g and percentage removal of 96.01%. The experimental data are well predicted by Pseudo Second Order (PSO) and Freundlich isotherm, indicating multilayer adsorption. The practicability and spontaneity of the adsorption process were confirmed through thermodynamic studies. A three-layer feedforward backpropagation network for the adsorption data was established using the Levenberg Marquardt training algorithm. The ANN model with structure 5-14-1, with Mean Square Error (8.01) and R^2 value (0.9823) was able to envisage good removal efficiency. It was concluded that the ANN model could predict the adsorption behavior of CQ on HSP1.

1. Introduction

Chloroquine (CQ), though a popular antimalarial drug, is often prescribed for the treatment of rheumatoid arthritis and in recent times, is used as a mild immunosuppressive (Schroeder & Gerber, 2014). CQ is one of the identified potent medications for the control of the COVID-19 pandemic and has since gained considerable attention due to its identified antiviral effect (Lei et al., 2020). Regardless of the questions arising from CQ's effectiveness in COVID-19 treatment, there has been a rise in demand for the drug (Abena et al., 2020; da Luz et al., 2021). The continuous use of CQ has led to a rapid rise in production, resulting from high demand and consequently leading to high concentrations in wastewaters (Dada et al., 2021).

Hotspots for CQ's release include pharmaceutical industrial wastewaters, hospital effluents, dumpsite leachate as well as unguided disposal of unused CQ medications (Bensalah et al., 2020; Dada et al., 2021). CQ is highly persistent due to its structural, chemical and physical properties, and as such can accumulate, pollute and become a serious threat to living organisms. CQ is highly water-soluble, hydrophilic and can prevail in the marine environment hence becoming a great concern (Babić et al., 2017). Most conventional wastewater treatment techniques are designed to eradicate solids, biodegradable organic materials, and suspended solids. Thus, various water pollutants are partially removed and concentrations of various others go with the discharged effluent. In some cases, concentrations of pollutants are high enough to raise a substantial level of environmental deterioration (Lindroos et al., 2019; Margot et al., 2015). Greater concern exists in developing countries, where untreated wastewaters are released into the environment (Kårelid et al., 2017; Lindroos et al., 2019; Singh et al., 2014). Adsorption wastewater treatment technique is found efficient for micro-pollutants removal and can help salvage the environment from the discharge of partially treated effluent. Therefore, if affordability is factored with the simplicity of adsorption technique, this may serve as a saving route for the developing nations' environment. Agricultural

* Corresponding author.
E-mail address: inyinbor.adejumoke@landmarkuniversity.edu.ng (A.A. Inyinbor).

https://doi.org/10.1016/j.sajce.2022.08.012
Received 28 June 2022; Received in revised form 10 August 2022; Accepted 31 August 2022
Available online 1 September 2022

Table 1
Isothermal model equations for adsorption of CQ onto HSP1 biochar.

Isotherms	Linear equation	Plot	Nomenclature of parameters and description	Reference
Langmuir	$\frac{C_e}{q_e} = \frac{C_e}{q_{max}} + \frac{1}{q_{max}K_L} R_L = \frac{1}{1+K_L C_e}$	C_e vs $\frac{C_e}{q_e}$	Ce represents the equilibrium concentration of CQ, q_e is the amount of CQ adsorbed at equilibrium, q_{max} is the maximum monolayer coverage (mg/g), K_L is the Langmuir isotherm constant (L/g), correlated to the binding energy of adsorption, R_L is the dimensionless separation factor indicating the favorability of adsorption.	(Langmuir, 1917)
Freundlich	$\log q_e = \log K_F + \frac{1}{n_F} \log C_e$	$\log C_e$ vs $\log q_e$	K_F is the indicator of Freundlich adsorption capacity, $\frac{1}{n_F}$ is the adsorption intensity correlating the surface heterogeneity and favorability of the process of adsorption.	(Freundlich, 1906)
Dubinin-Radushkevich	$lnq_e = lnq_m - A_{DRK}\varepsilon^2$ $\varepsilon = RTln\left[1 + \frac{1}{C_e}\right]$ $E = -\left[\frac{1}{\sqrt{2A_{D-R}}}\right]$	ε^2 vs lnq_e	q_m is the adsorption isotherm (theoretical) saturation capacity (mg/g), A_{DRK} is the D-R constant (mol^2/kJ^2). ε is the Polanyi potential, E is the mean free adsorption energy which predicts the adsorption nature (chemisorption or physisorption).	(Dubinin & Radushkevich, 1947)
Temkin	$q_e = \frac{RT}{b_T} lnA_T + \frac{RT}{b_T} lnC_e$	lnC_e vs q_e	bT is the Temkin constant relating to heat of adsorption, AT is the Temkin binding constant at equilibrium (L/g), R is the universal gas constant (8.314 J/mol/K), $B = RT/b_T$ is the constant related to the heat of adsorption (J/mol).	(Ringot et al., 2007)
Redlich-Peterson	$ln\frac{C_e}{q_e} = BlnC_e - lnA$	lnC_e vs $ln\frac{C_e}{q_e}$		
Hasley	$lnq_e = \frac{1}{n_H} lnK_H - \frac{1}{n_H} lnC_e$	lnC_e vs q_e	K_H and n_H are Hasley's isotherm constant and exponent respectively.	(Belhachemi & Addoun, 2011)
Hill	$log\frac{q_e}{q_H - q_e} = n_H log C_e - logK_D$	$logC_e$ vs $log\frac{q_e}{q_H - q_e}$	K_D, q_H and n_H are Hill's isotherm constants.	(Hamdaoui & Naffrechoux, 2007)

Table 2
Kinetics model equations for adsorption of CQ onto HSP1 biochar.

Isotherms	Linear equation	Plot	Nomenclature of parameters and description	Reference
Pseudo-first order	$\log(q_e - q_t) = lnq_e - K_1 t$	t vs $\log(q_e - q_t)$	q_e is the quantity of CQ removed at equilibrium (mg/g), q_t is the quantity of CQ adsorbed at the time, t (mg/g), K_1 is the rate constant of PSO (m^{-1}) and t is time (min).	(Lagergren, 1898)
Pseudo-second order	$\frac{t}{q_t} = \frac{1}{K_2 q_e^2} + \frac{t}{q_e}$	t vs $\frac{t}{q_t}$	K_2 is the rate constant of pseudo second order (g/mg/min).	(Ho & McKay, 1998)
Elovich	$q_t = \frac{1}{\beta}\ln(\alpha\beta) + \frac{1}{\beta} lnt$	t vs q_t	α is the constant related to the rate of chemisorption and β is the constant that depicts the extent of the surface coverage.	(Aharoni & Ungarish, 1976)
Avrami	$ln\left[\ln\left(\frac{q_e}{q_e - q_t}\right)\right] = nlnK_{AV} + nlnt$	t vs $ln\left[\ln\left(\frac{q_e}{q_e - q_t}\right)\right]$	n is the Avrami model exponent of time relating to change in adsorption mechanism, while K_{AV} is the Avrami constant.	(Lopes et al., 2003)
Intraparticle diffusion	$q_t = K_{Diff} t^{0.5} + C$	$t^{0.5}$ vs q_t	K_{Diff} is the rate constant for Intraparticle diffusion (mg/g min$^{-1/2}$), C profers the insight into the boundary layer thickness.	(Weber & Morris, 1963)
Liquid film diffusion	$\ln\left(1 - \left(\frac{q_t}{q_e}\right)\right) = -K_{LFD} t + C$	t vs $\ln\left(1 - \left(\frac{q_t}{q_e}\right)\right)$	K_{LFD} is the coefficient rate for the process corresponding to Hsp1 particle size.	
Fractional power	$\log(q_t) = \log(K) + vlot(t)$	t vs$\log(q_t)$	v is a positive constant < 1, K is a constant.	

Table 3
Statistical error validity.

Statistical error validator	Equation	Nomenclature of parameters and description	Reference
Chi square (X^2)	$\sum_{i=1}^{n} \frac{(q_{e,exp} - q_{e,cal})}{q_{e,cal}}$	N is the number of the data point, $q_{e,exp}$ and $q_{e,cal}$ (mg/g) are the experimental and calculated quantity adsorbed. A lower value in error analysis indicated a good fit between the calculated and the experimental data	
Standard deviation (S.D (%))	$100\ X \left\{\frac{\{\sum_N (1 - (q_{t,cal}/q_{t,exp}))^2\}}{N}\right\}^{1/2}$		(Inyinbor et al., 2019)
Average relative error (ARE)	$\frac{100}{n}\sum_{i=1}^{n}\left\|\frac{(q_{e,cal} - q_{e,exp})}{q_{e,exp}}\right\|$		(Prasad et al., 2015)

waste may satisfactorily fill the economical gap in adsorption techniques hence our quest.

A large part of agricultural wastes is composed mainly of lignin, hemicellulose and cellulose. These components are the structural materials embedded within the multifaceted architecture of plant cell walls. Reports have shown that the presence of lignin and cellulose in material influences the properties/performances of the resulting adsorbent (Xue et al., 2018). *Hibiscus sabdariffa* seed pods are an underutilized agro-waste, that is rich in cellulose (Adewuyi & Vargas Pereira, 2017), hence, can serve as a good precursor for adsorbent preparation. Different modeling techniques can be used to evaluate the efficiency of an adsorption process. One of such models is Artificial Neural Network (ANN). ANN is an artificial intelligence, inspired by studies carried out on the structure and function of the brain and the nervous system. The

Table 4
Total number of parameters used in the development of the ANN model for kinetics of CQ removal unto HSP1.

Type	Information/ Remarks	Selection mode
Input layer	5 neurons	Based on number of input variables
Hidden layer	14 neurons	Comparison of 1-20 neurons
Output layer	1 neuron	Based on number of output variable
Total datasets used in training	1,180	Random division
Total datasets used for testing	252	Random division
Total datasets used for validating	252	Random division
Number of transfer function	3	

Table 5
Input variables range used in the development of the ANN model for kinetics of CQ removal unto HSP1.

Parameters	Range
CQ initial concentration	5,10,20,30,40 and 50
pH	2,3,4,5,6,7,8,9 and 10
Temperature	299, 308, 318 and 328
Contact time	1,5,10,15,20,25,30,60,120…
Dosage	0.04, 0.08, 0.12, 0.16 and 0.20

ANN model incorporates the course of learning and response (Khan et al., 2017). ANN had been used to solve several multifaceted engineering problems (Afolabi et al., 2020a; Kavitha & Sarala Thambavani, 2020; Khan et al., 2017; Pauletto et al., 2021b). The wide applicability of ANN is due to its robustness, simplicity, nonlinearity and reliability (Khalili et al., 2021). According to reports, in the use of artificial intelligence, when there is an agreement between the material design and the discovery. It saves costs and time required for laboratory practical applications. This in turn can greatly improve the efficiency of the research processes (Shuaihua et al., 2018; Wang et al., 2021; Yuan et al., 2018).

Herein, we prepared a cost-friendly and effective biochar from *Hibiscus sabdariffa* seed pods (HSP1). Acid activation was carried out to enhance the pores, increase the surface area and enhance the number of active sites on the prepared adsorbent. An extensive characterization via different physicochemical and spectrophotometric techniques was investigated on HSP1. Prepared HSP1 was employed for CQ scavenging. To the best of our knowledge, the adsorption of CQ using *Hibiscus sabdariffa* seed pods (green roselles) has not been previously reported hence, a novelty. Additionally, the complex relationship between the prepared adsorbent and CQ was monitored using the ANN model. For the first time, different ANN architectures that could optimally predict CQ adsorption efficiency onto HSP1 adsorbent were investigated. Different hidden neurons and activation functions were compared. The experimental data were also simulated to estimate the adsorption efficiency. The optimum ANN model was predicted via regression coefficients and root mean square error.

2. Experimental

2.1. Development of HSP1 biochar

Hibiscus sabdariffa seed pods were obtained from local farmers in Omu Aran, Kwara State, Nigeria. The waste material was properly

Table 6
Physical properties of HSP1 biochar.

PROPERTY	HSP	HSP1
pH	6.01±0.02	6.01±0.02
pH_{pzc}	4.00±0.02	3.20±0.02
Micropore volume (cm^3/g	0.152	0.152
Average pore volume (nm)	3.253	2.856
BET surface area (m^2/g)	990.52	994.55
Langmuir surface area (m^2/g)	980.3	984.34
Iodine surface area (m^2/g)	715.33	925.29
Bulk density (g/cm^3)	0.192	0.322
% Moisture	8.31	3.20
% Volatile matter	16.52	10.33
% Ash	12.83	8.30
% Fixed carbon	62.34	78.17

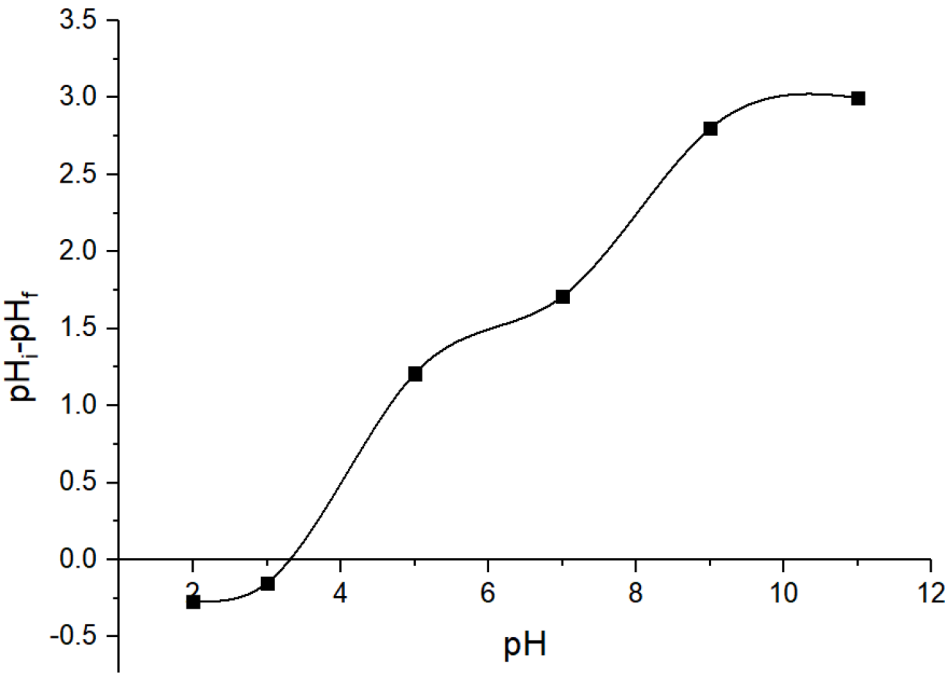

Fig. 1. Isoelectric point of HSP1 biochar.

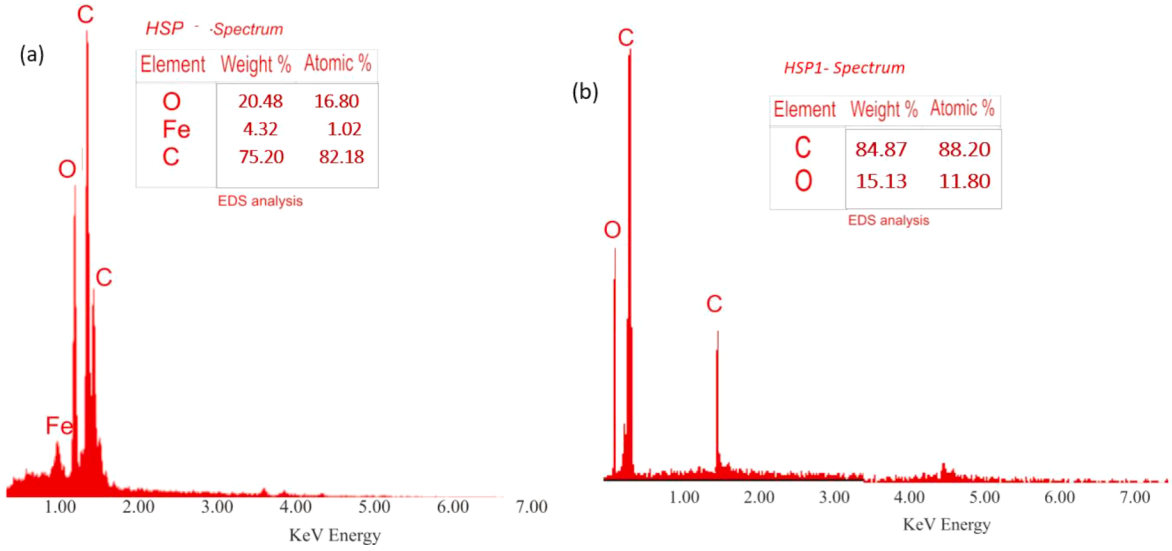

Fig. 2. Elemental composition of (a) HSP (b) HSP1.

Table 7
Determination of oxygen containing groups in HSP1.

Groups	HSP1
Lactones (mmol g^{-1})	0.909
Carboxylic (mmol g^{-1})	-
Phenols (mmol g^{-1})	4.091
Acidic sites (mmol g^{-1})	5.00
Basic sites (mmol g^{-1})	0.682

washed to eradicate dirt using deionized water. The cleaned material was then dried in the oven at 105 °C for 24 hours. The dried sample was milled to a particle size of 250 μm and initial activation with ortho-phosphoric acid was done. This was achieved by contacting the sample with 98 % orthophosphoric acid, heated for 90 minutes at 105 °C with continuous stirring until a paste was formed. The paste was then transferred to the furnace and carbonized at 350 °C for 90 minutes. The developed char was then washed severally with deionized water to a neutral pH and dried at 105 °C for 24 hours. The prepared adsorbent was stored in a well-sealed container and labeled HSP1.

2.2. Characterization techniques for HSP1 biochar

HSP1 was analyzed for the physicochemical properties which include pH, moisture percent, ash percent, volatile matter, bulk density, BET surface area by iodine number, Boehm titration, and pH point of zero charge. This was achieved following the procedures reported by (Dada et al., 2021; Ekpete et al., 2017). BET analysis was carried out to examine the surface area of HSP1. FTIR spectroscopy was used to identify the variations that took place in the vibrational frequency of the functional groups in HSP1. EDX analysis was carried out to estimate the percentage, oxygen content and other elements present in HSP1. The topography and surface morphology were analyzed using SEM, with the focus set at 10.0 kV and an image magnification of 500 was chosen for discussion.

2.3. Adsorption studies of the removal of CQ onto HSP1 biochar

A CQ stock solution of 100 ppm was prepared by dissolving 0.1g in 1 L of deionized water. Several working concentrations were prepared via serial dilutions. Batch adsorption studies were carried out by introducing 0.1g of HSP1 to 100 mL solution of different CQ concentrations (5 – 50 mg/L). The sample containing the aqueous solution was then agitated on a mechanical shaker (SHA-C water bath shaker) at 150 rpm. The solutions were removed at a predetermined time and analyzed using a Biochrome Libra 160 UV-visible spectrophotometer. The effect of pH (1-12), contact time, CQ initial concentration (5-50 ppm), HSP1 dosage (0.04 -0.20 g/L) and temperature (299 – 328 K) were explored. The pH of the working solutions was adjusted using 0.1 M NaOH and HCl reagents.

2.4. Adsorption Kinetics, Isotherms and Statistical validity error

The experimental data obtained from this study were subjected to seven different isotherm models which include Langmuir, Freundlich, Temkin, Dubinin-Radushkevich, Redlich-Peterson, Hasley and Hill models. Also, the mechanism and kinetic data were fitted to Pseudo first order, Pseudo second order, Elovich, Intraparticle diffusion, Liquid film diffusion, Fractional power and Avrami models. The percentage removal and quantity adsorbed were estimated using Eqs. (1) and (2) respectively.

$$\%\ Removal = \frac{(C_o - C_e)}{C_o} \text{x } 100 \tag{1}$$

$$q_e = \frac{(C_o - C_e)v}{w} \tag{2}$$

The determination of the best fit for the kinetic and isotherm models has regularly been done through the application of R^2 (linear correlation coefficient). Due to the bias of the results, Chi-square (X^2), Average relative error (ARE) and the standard deviation (S.D %) were used in addition to the correlation coefficients. The full description of the isotherms, kinetic models and statistical validity of error are presented in (Tables 1, 2 and 3).

2.4. Desorption studies on HSP1 biochar

The desorption process was executed by adding 0.1 g of CQ loaded HSP1 to 40 mL of 0.1 M Deionized water, NaOH, HCl and NaCl solutions as desorbing agents and agitated on a mechanical shaker for 90 minutes. The temperature was maintained at 26 °C and the percentage desorption efficiency was calculated using Eq. (3).

$$Desorption\ efficiency\ (\%) = \frac{q_{de}}{q_{ad}}\ X\ 100 \tag{3}$$

q_{de} and q_{ad} represent the desorbed and adsorbed quantity respectively.

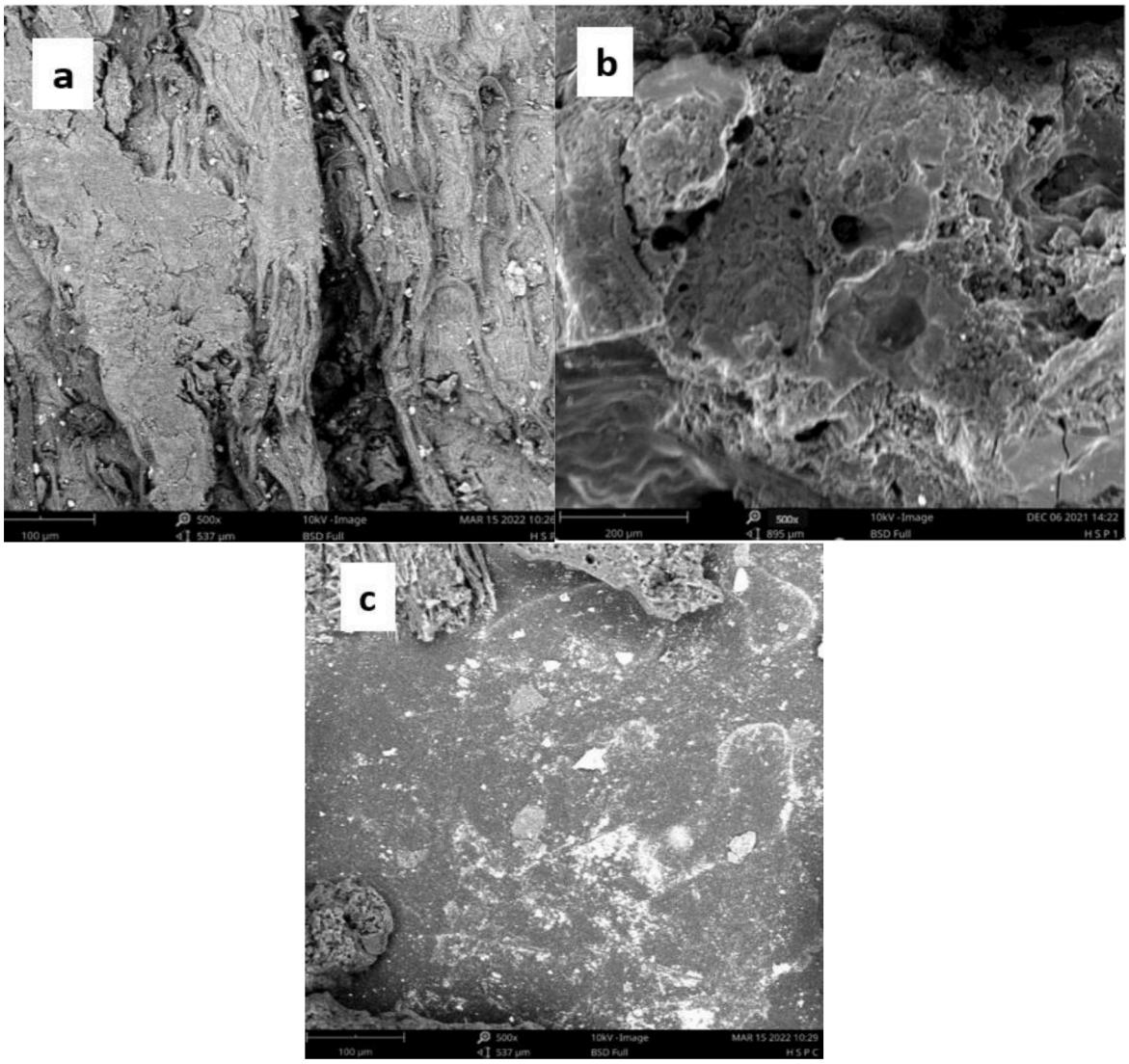

Fig. 3. SEM morphologies of (a) raw HSP (b) acid activated HSP before adsorption (c) HSP1 after adsorption.

2.5. Artificial neural networks (ANN) model estimation of HSP1 adsorption efficiency

In this study, the algorithms and architecture to be used was selected based on several iterations, as there has been no developed standard approach for the selection (Afolabi et al., 2020b, 2020a; Khan et al., 2017). A three-layer backpropagation neural network was employed using MATLAB (2016a) mathematical software. The summary of parameters and input variables range employed in the development of the ANN model for the kinetics of CQ removal unto HSP1 is presented in (Tables 4 and 5) respectively.

3. Results and discussion

3.1. Characterization of HSP1 biochar

The pH_{pzc} (isoelectric point) which explores the surface charge of HSP1 was found to be 3.20 (acidic) as shown in Fig. 1. The positive surface of HSP1 will offer affinity for anionic species. CQ have pKa values of 4.0, 8.4 and 10.2 which means that CQ can exist as anionic species with built attraction for the cationic HSP1 (Schroeder et al., 2015; Bello et al., 2017; Inyinbor et al., 2022a).

The physical properties of HSP1 are presented in Table 6. The raw HSP pod were observed to have high moisture and volatile matter which decreased greatly after activation. During the application of heat, the bonds of the organic components break, causing the organic molecules to be unstable. The process of activation coupled with carbonization helps to eradicate the moisture level and volatile matter, leaving a carbon-rich sample. The elemental composition analysis also revealed an increase in carbon content of HSP after the acid activation as shown in Fig. 2a and b. The carbon content increased from 75.20 % to 84.87%. Carbon-rich adsorbents have been described as an effective remediation material for various contaminants/pollutants removal (Bello et al., 2021).

The adsorption of iodine was carried out to determine the surface area and was found to increase from 715.33 and 925.29 m^2/g for raw and activated HSP1 respectively. These values agree with the surface area derived from the BET analysis which also increased from 980.3 to 984.34 m^2/g. In addition, the average pore volume of HSP1 (2.856 nm) which is greater than 2 nm but less than 50 nm classified HSP1 as a mesoporous biochar hence suitable for the uptake of large molecules such as CQ. Availability of high surface area and abundant pores on HSP1 are indicators of effective adsorbents (Ekpete et al., 2017; Pauletto et al., 2021a; Thommes et al., 2015).

Boehm titration provides semi-quantitative information about the sum total of oxygen-bearing groups on HSP1 surface. The detailed

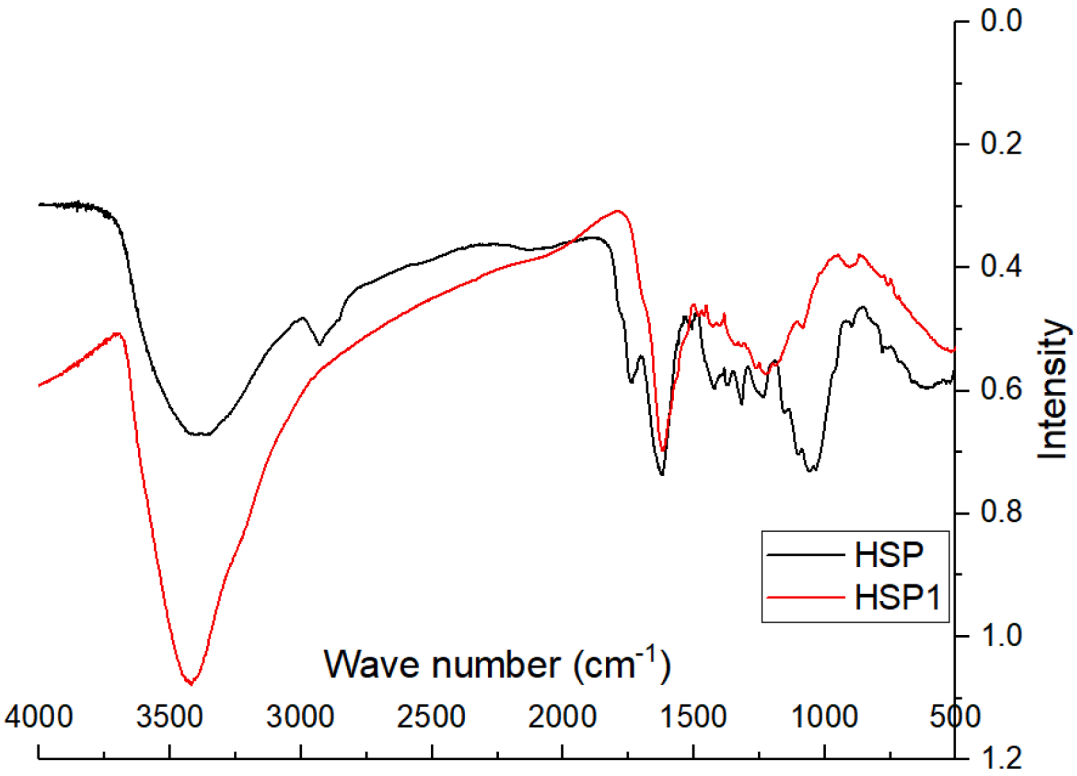

Fig. 4. FTIR spectra of raw and activated HSP adsorbents.

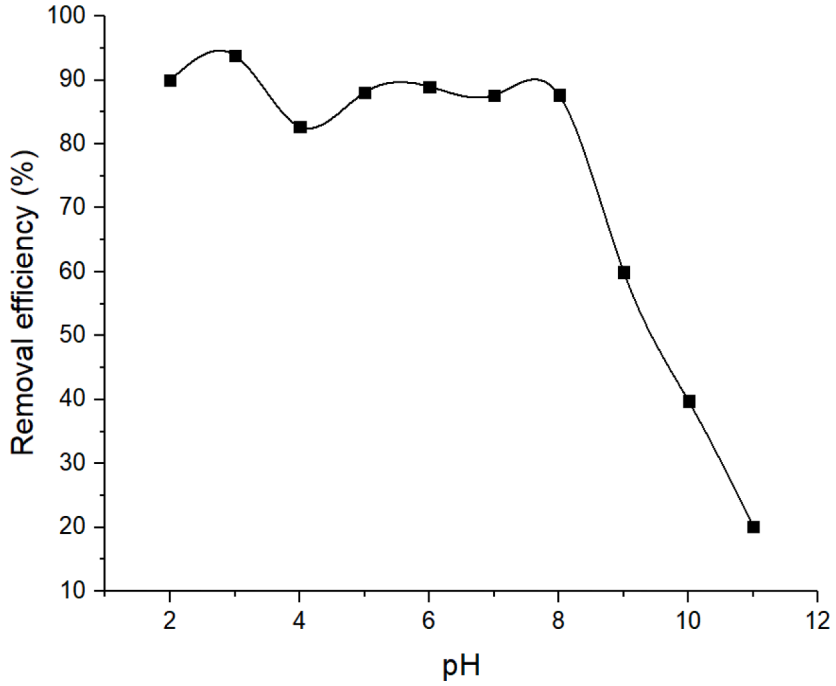

Fig. 5. Effect of pH on CQ uptake onto HSP1 (Conditions: contact time (4 hours), initial concentration (30 ppm), dosage (1 g/L), temperature (26 °C), pH (3).

findings are revealed in (Table 7). It was noted that HSP1 biochar contains higher number of acidic sites than the basic sites which corresponds with the isoelectric point value obtained for HSP1.

Fig. 3a, b and c presented the surface morphologies of HSP1 Before activation, before adsorption and after adsorption. The surface of raw HSP1 appears to be wood-like with no distinct pore opening. Several large pronounced pores were visible after activation (Fig. 3b). This could be attributed to the breakdown in lignocellulosic materials due to the high temperature applied and the elimination of volatile matter (Auta & Hameed, 2011). However, there was an observable blockage in the pores of HSP1 after CQ adsorption (Fig 3c), which indicated that the pores have been filled up with CQ molecules.

The FTIR spectroscopy which helps to identify functional groups was analysed. The availability of different functional groups greatly

Table 8
ANOVA data for adsorption capacity of CQ onto HSP1 activated biochar.

Source	Sum of Squares	df	Mean Square	F-value	p-value	
Model	1378588.448[a]	35	39388.241	1189.745	.000	significant
Concentration	18314.611	6	3052.435	92.201	.000	
dosage	748.064	5	149.613	4.519	.001	
pH	7668.021	9	852.002	25.735	.000	
Time	162418.524	11	14765.320	445.995	.000	
Temperature	4786.956	3	1595.652	48.198	.000	
Error	9038.065	273	33.106			
Total	1387626.513	308				

a. R Squared = .993 (Adjusted R Squared = .993)

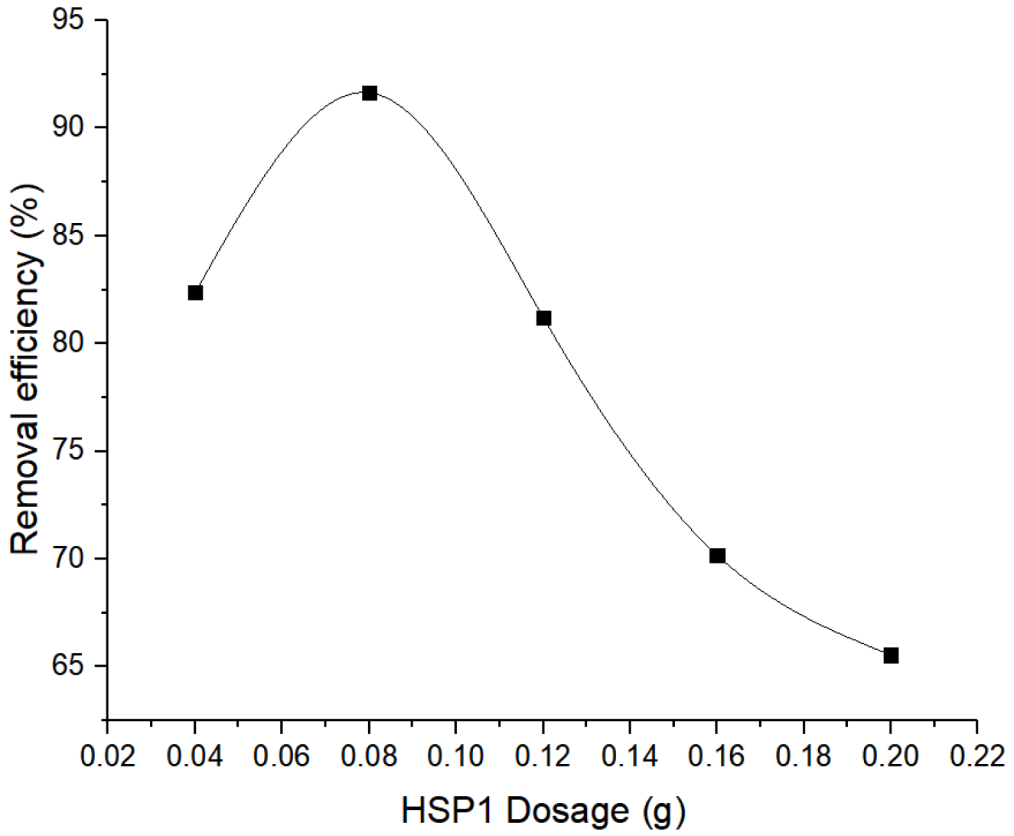

Fig. 6. Effect of dosage on CQ uptake onto HSP1 (Conditions: contact time (4 hours), initial concentration (30 ppm), temperature (26 °C), pH (3).

contributes to pollutants removal form wastewaters. Fig. 4 showed the FTIR bands of raw and activated HSP, slight shift in the peak values were observed. This could be attributed to the development of chemical bonds between HSP1 functional groups. Broad bands observed at 3,392.17 and 3404.71 cm^{-1} for the raw and activated material represent the bonded OH functional groups. Bands observed at 2925.97 cm-1 for the raw HSP represents the C-H aliphatic. The peak at 1615.09 to 1617.50 cm^{-1} represents C=O stretch and the peak at 1212.04 cm^{-1} was assigned to -SO_3 stretching group. The band at 1033.66 cm^{-1} corresponds to C=O bond of ester, phenol or ether. The band at 586.25 cm^{-1} corresponds to S-O. The observable variations in the spectra established the effect of acid activation (Bello et al., 2017; Obayomi et al., 2021).

3.2. Effect of operational parameters

3.2.1. Adsorption mechanism of CQ uptake onto HSP1

A very important parameter that governs the process of adsorption is the pH. The adsorption sites as well as the adsorbate properties is generally affected by the pH . As observed in Fig. 5, there was an initial increase in the percentage removal of CQ onto HSP1 (87.66 -93.87 %) from pH 2 to 3, followed by a slight reduction (93.87 to 86.66 %) from pH 3 to 8. A sharp reduction in the percentage removal (86.66 – 20.19 %) from pH 9-11. The optimum pH was recorded for pH 3 which can be attributed to a change in CQ medium at different pH levels. pH changes often result in the development of diverse ionic species. Features like nature of functional groups, hydrophobicity and pKa of the adsorbate and the surface charge as well as functional groups on the adsorbent can influence the adsorption process (Pauletto et al., 2021a). CQ have three pKa values 4.0, 8.4 and 10.2 (strong base) (Schroeder & Gerber, 2014). This could explain why CQ have high percentage removal over a wide range of pH (3-8). A possible mechanism of reaction between CQ molecules and HSP1 adsorbent is the Hydrogen bonding interaction. The -OH groups on HSP1 can serve as hydrogen donor whereas the Nitrogen atoms on CQ can act as hydrogen acceptors. This type of interaction is termed dipole-dipole hydrogen bonding. The drop in the percentage removal from pH 9-11 could be due to electrostatic repulsion as a of excess negatively charged ions (Fakhri, 2017). The ANOVA analysis at 95% degree of freedom (Table 8) was performed. Factors like Dosage, concentration, pH, time and temperature have a significant effect on the percentage CQ removal.

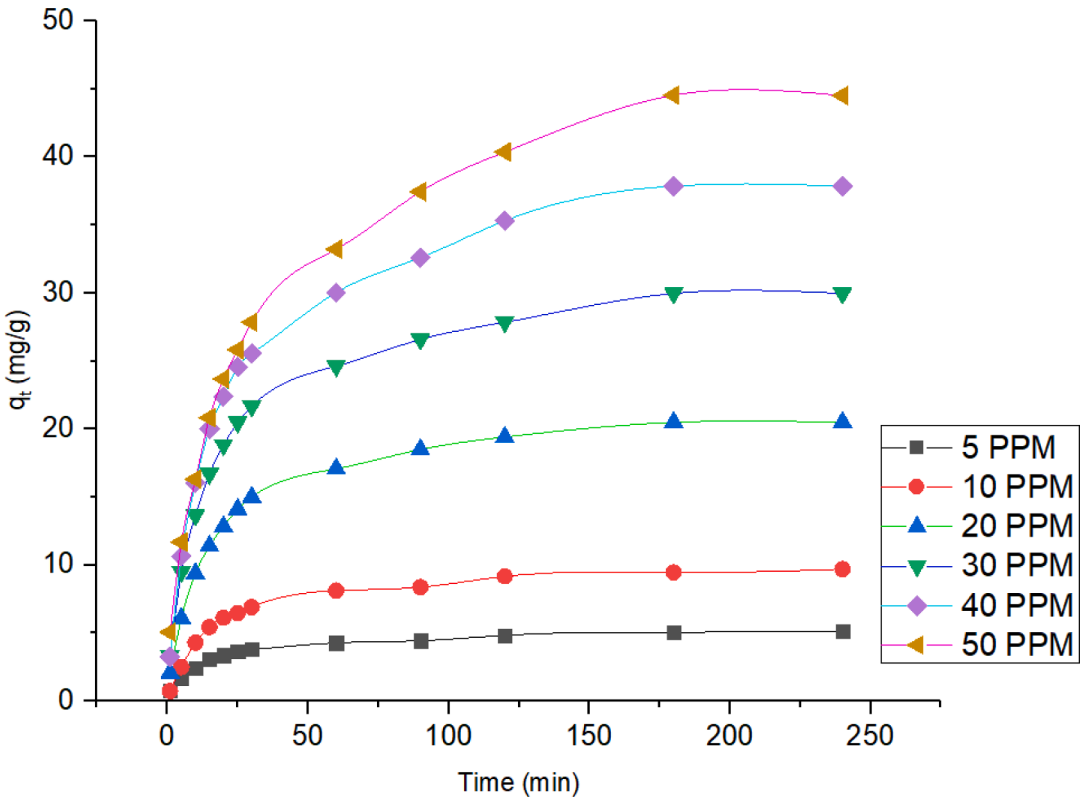

Fig. 7. Effect of initial concentration and contact time on CQ uptake onto HSP1 (Conditions: temperature (26 °C), pH (3), dosage (1 g/L).

Table 9
Kinetic models for the adsorption of CQ unto HSP1.

Kinetic models	Parameters	Concentration (mg/L)					
		5	10	20	30	40	50
	q_e Exprimental (mg/g)	5.15	9.69	20.49	29.97	37.85	44.55
Pseudo first order	q_e Calculated (mg/g)	36.11	163	929.82	4671.97	5436.26	35164.14
	$K_{1\ x}\ 10^{-2}$ (min^{-1})	9.61	7.65	8.11	10.57	8.51	12.81
	R^2	0.7909	0.8944	0.8952	0.8832	0.9084	0.8539
	S.D (%)	245.21	645.69	1811.71	6323.43	5822.27	32183.63
	X^2	26.54	144.19	889.29	4612.22	5360.82	35075.09
	ARE	100.11	263.61	739.63	2581.53	2376.93	13138.91
Pseudo second order	q_e Calculated (mg/g)	5.41	10.29	21.65	31.55	40.32	47.85
	$K_{2\ x}\ 10^{-3}$ (g/mg/min)	9.74	6.58	3.52	2.41	1.54	1.09
	R^2	0.9977	0.9991	0.9994	0.9989	0.9985	0.9959
	S.D (%)	0.9634	1.1757	1.0665	0.9994	1.2251	1.3785
	X^2	0.0126	0.0356	0.0615	0.0788	0.1513	0.2273
	ARE	0.8435	1.0409	0.9388	0.8767	1.0875	1.2338
Avrami	n_{AV}	0.7343	0.8087	0.7683	0.7776	0.7887	0.8574
	K_{AV} (min^{-1})	0.7000	0.7234	0.7169	0.7141	0.7271	0.7209
	R^2	0.9731	0.9856	0.9684	0.9385	0.9591	0.9191
Elovich							
	α_{EI} (mg/g.min)	0.8333	0.5631	0.2646	0.1862	0.1464	0.1251
	β_{EI} (g/mg)	0.0025	0.3264	0.5374	0.5431	0.7373	0.8993
	R^2	0.9777	0.9812	0.9875	0.9902	0.9902	0.977
	S.D (%)	16.6667	16.6478	16.6552	16.6612	16.6603	16.6599
	X^2	10502.06	268.81	740.93	1594.41	1868.36	2118.61
	ARE	16.6585	16.1055	16.2296	16.3646	16.3421	16.3302
Intraparticle diffusion	K_{diff} (mg/g $min^{-1/2}$)	0.3958	0.6626	1.3704	1.9511	2.5715	3.0721
	C_I (mg/g)	1.1681	2.1405	4.9879	7.5334	7.8588	7.4137
	R^2	0.8755	0.8454	0.8522	0.8578	0.8855	0.9403
	S.D (%)	99.14	99.19	99.01	98.95	99.28	99.54
	X^2	13.59	26.65	48.18	66.82	114.48	186.01
	ARE	56.86	58.81	51.81	49.64	63.61	83.48

(*continued on next page*)

Table 9 (*continued*)

Kinetic models	Parameters	Concentration (mg/L)					
		5	10	20	30	40	50
Liquid film diffusion	K_{FD}	0.0287	0.0275	0.0292	0.0257	0.032	0.0512
	R^2	0.9489	0.9684	0.9706	0.9685	0.9407	0.9341
Fractional power	V (min^{-1})	0.2912	0.4355	0.3913	0.3754	0.4164	0.3931
	K (mg/g/hr)	1.2847	1.2627	3.2441	5.0351	5.2095	6.375291
	R^2	0.9088	0.8698	0.8903	0.8969	0.8979	0.9595
	X^2	11.65	56.29	91.6874	123.4795	204.54	228.58
	S.D (%)	12.51	14.49	14.03	13.87	14.372	14.28
	ARE	12.51	14.49	14.03	13.87	14.373	14.28

3.2.2. *Effect of HSP1 dosage*

Fig. 6 depicts the experimental results that distinguished the effect of HSP1 dosage on CQ removal. The findings revealed that there was an initial increase in percentage removal as the dosage increased from 0.04 to 0.08 g/L, due to the availability of more sites for adsorption. A decrease in adsorption efficiency was however observed beyond HSP1 dose of 0.08g/L due to aggregation of the adsorbent (Al-Ghouti & Al-Absi, 2020; M & G, 2020).

3.2.3. *Effect of initial concentration and contact time on CQ removal onto HSP1*

This factor has a lot to do with immediate interaction between the available binding sites on HSP1 and CQ concentration. There was an initial increase in adsorption rate as shown in Fig. 7. However, over time, the process slowed down and became constant as a result of saturated HSP1 surface. Similar trends have been reported in literature (Dada et al., 2021; Inyinbor et al., 2022a; Obayomi et al., 2021).

3.2.4. *Effects of temperature on the uptake of CQ unto HSP1*

Different temperatures (299, 308, 318 and 328 K) were investigated. The observed results from batch studies showed highest adsorption occurred at 328 K with 96.01% at equilibrium time of 120 minutes. Also, at 299 K, a percentage removal of 93.93% was observed under the same operation conditions, which equally favoured the adsorption process. The percentage removal increased with increased temperature suggesting an endothermic adsorption process (Al-Ghouti & Al-Absi, 2020).

3.3. *Adsorption kinetic models*

The effects of time of contact on the adsorption of CQ unto HSP1 at different concentrations (5 -50 mg/L) are presented in Fig. 7. Seven different kinetic models were used to fit the adsorption data as presented in (Table 9). The PSO model displayed a brilliant fit, with the correlation coefficient ranging between 0.9959 and 0.9994. This prediction was further confirmed by estimated low error values (ARE, S.D % and $\Delta q_{e.}$). This is an indication that the rate limiting step is chemisorption (Amin et al., 2015). The correlation coefficient of the Liquid film diffusion model ranges between 0.9341 and 0.9701, which shows the significance of film diffusion as a contributing factor to determining rate. Also the increase in K_{fd} values across the investigated concentrations indicate that increase in concentration sped up the adsorption rate (Tarawou & Young, 2015). The Fractional power plot shows that the values of K and V are positive, increases with increase in concentration and greater than one, indicating a rapid kinetic process (Ojediran et al., 2021). Intra-particle diffusion seem not to be the only rate determining step as the plot of q_t versus $t^{1/2}$ did not go through the origin. The values of C, are however greater than zero across all the investigated concentration. This an indication that there is a participation of the boundary thickness in the adsorption processes and the rate-controlling step involves another diffusion model (Dehbi et al., 2020).

3.4. *Adsorption isotherms for CQ uptake onto HSP1*

The Freundlich, Langmuir, Temkin, Dubinin-Radushkevich, Hasley, Hill and Redlich-Peterson isotherms were applied in this study. The correlation coefficient values obtained for each of the isotherms are concise in (Table 10). The adsorption of CQ unto HSP1 proposed a multilayer adsorption with the highest R^2 values (up to 0.9995). The values of n which describe the intensity and the feasible the adsorption processes were observed in the range 1 – 10 (Dada et al., 2021). This was in turn confirmed by the Hasley isotherm. The dimensionless separation factor, R_L was found to be greater than zero but less than one (0.0338 - 0.5945), across all the investigated temperatures. This is an indication that the adsorption process was favourable. The Temkin equilibrium binding constant A_T (8.7199 L/g), the constant relating to heat of

Table 10
Isotherm parameters for the adsorptive removal of CQ unto HSP1.

Isotherm models	Parameters				
Temperature (K)		299	308	318	328
Freundlich	K_F	11.8195	8.1846	10.2023	17.5873
	n	1.5672	1.3459	1.1506	1.7724
	R^2	0.9862	0.9969	0.9995	0.9868
Langmuir	K_L (L/mg)	0.571	0.0895	0.0682	0.5093
	q_{max} (mg/g)	50.76	80	161.29	60.98
	R_L	0.149 - 0.0338	0.5278 - 0.2714	0.5945 - 0.2267	0.1641 - 0.03785
	R^2	0.8997	0.7151	0.9413	0.9265
Temkin	B	9.7838	8.4415	16.214	16.009
	A_T (L/g)	7.6522	8.7199	1.9896	3.7733
	bT (KJ/mol)	262.58	303.35	163.06	170.34
	R^2	0.992	0.9532	0.9804	0.9994
D-R	q_{DR} (mg/g)	39.1461	49.5162	42.83	42.43
	β x 10^{-7}($mmol^2J^{-2}$)	1	10	3	2
	R^2	0.9961	0.9908	0.9926	0.9294
Hasley	K_H	11.8189	8.1846	10.2022	17.5895
	n_H	1.5672	0.8749	1.1506	1.7724
	$^1/n_H$	0.6381	1.143	0.8691	0.5642
	R^2	0.9862	0.9962	0.9995	0.9768
R-P	a_R (L/mg)	11.8289	4.9185	10.2011	17.5895
	B	0.3619	0.137	0.1309	0.4358
	R^2	0.9583	0.947	0.9767	0.9618
Hill	n_H	1.3934	1.1875	0.975	1.2792
	K_D	0.3999	0.3801	0.0558	2.1787
	q_H	50.76	80	161.29	60.98
	R^2	0.9784	0.8664	0.9735	0.9826

Table 11
Thermodynamic parameters for the adsorption of CQ unto HSP1.

Temp. (K)	ΔS^o (JK^{-1} mol^{-1})	ΔG^o (KJ mol^{-1})	ΔH^o (KJ mol^{-1})
299		-2.77	
308	108.91	-3.62	29.88
318		-4.64	
328		-5.96	

Table 12
Comparison of the monolayer adsorption capacity of CQ onto HSP1.

Adsorbate	Adsorbent	q_{max} (mg/g)	Reference
	Edible clay	2.14	
	Aluminium hydroxide	3.91	(Iwuagwu & Aloko, 1992)
Chloroquine	Magnesium oxide	4.18	
	Magnesium trisilicate	4.72	
	Plantain peel nanoparticle	50.51	(Dada et al., 2021)
	This study 161.29		This study

adsorption, b_T (262.58 KJ/mol) and the correlation coefficient (0.9994), indicating a chemical adsorption. Relatively low correlation coefficient and high error values obtained for Langmuir and Hill isotherms compared to other investigated isotherms shows that these models do not suitably fit the adsorption data. The maximum adsorption capacity of HSP1 was compared with the q_{max} previously reported in literature (Table 11). The reported data were limited, however HSP1 revealed a better performance Fig. 8.

3.5. Thermodynamic studies of CQ uptake onto HSP1

The values obtained for thermodynamic parameters is presented in (Table 11). The positive value of ΔH^o obtained for the removal of CQ unto HSP1 showed that the adsorption process is endothermic in nature. The negative values of ΔG^o predicted that the adsorption of CQ unto HSP1 is feasible and spontaneous (Al-Ghouti & Al-Absi, 2020; Dada et al., 2021; Inyinbor et al., 2022a). Moreso, the negative values ΔG^o of increases as the temperature increases, indicating that the adsorption process is favourable at higher temperatures (Kaur et al., 2012). The value of ΔS^o is positive which suggests that randomness in the adsorption system Table 12.

Table 13
Statistical metrics for selection of hidden neurons.

Hidden neurons	MSE	R^2
1	44.48	0.93026
2	25.12	0.961969
3	20.03	0.976539
4	18.39	0.976342
5	20.42	0.976737
6	20.08	0.97338
7	14.89	0.979308
8	13.36	0.974169
9	13.27	0.975156
10	9.08	0.988235
11	11.98	0.978714
12	11.11	0.985056
13	11.21	0.981883
14	8.01	0.987241
15	11.35	0.981486
16	10.15	0.982279
17	11.81	0.981685
18	11.73	0.980892
19	13.99	0.975156
20	13.53	0.978319

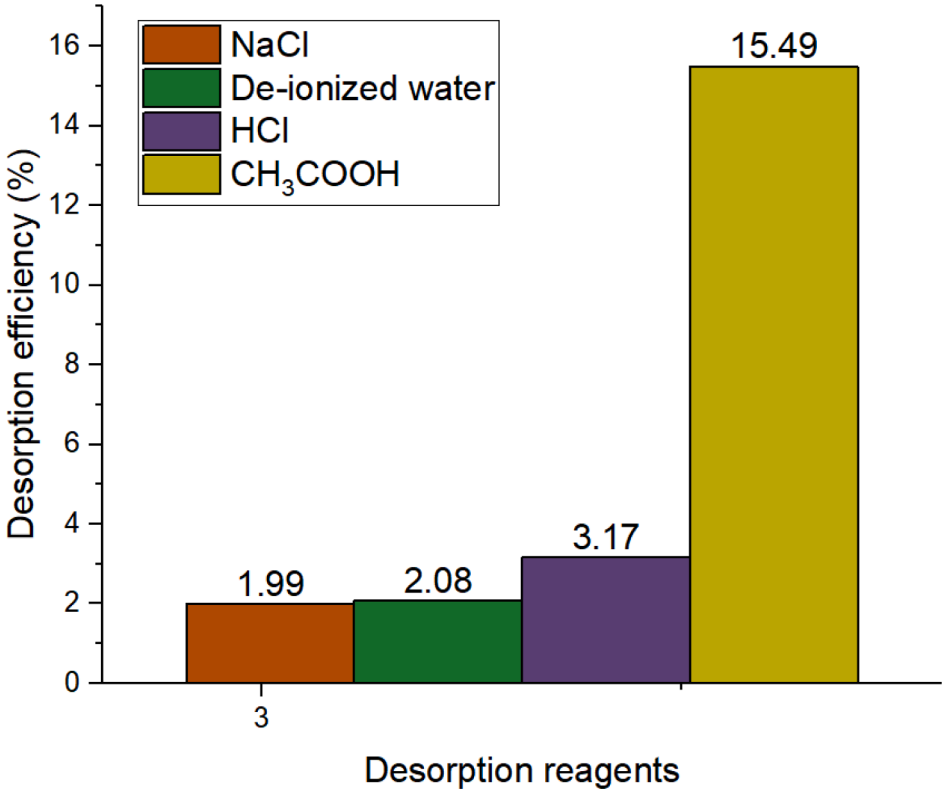

Fig. 8. Desorption efficiency of HSP1.

3.6. Desorption studies of HSP1

The desorption efficiency was recorded in this order; CH_3COOH>HCl>NaOH>NaCl>H_2O (15.49>4.06%>3.36%>2.12%> 2.10%). The desorption efficiency (Fig. 7) was observed to be generally low which suggests that CQ penetrates the pore of HSP1. As reported, several contact points can establish a large net adsorption between and adsorbents. This can make CQ release very difficult (Fernandez et al., 2010; Inyinbor et al., 2015). Hence chemisorption governs the adsorption mechanism. The wide availability of *Hibiscus sabdariffa* plant can however atone for its economical use as adsorbent.

Table 14
Comparison of activation function.

Transfer function	R^2
Logsig	0.991817
Purelin	0.83869
Transig	0.82283

3.7. Result OF Artificial Neural Network Model (ANN)

3.7.1. Determination of optimal number of hidden neurons

The optimal number of hidden neurons is very crucial, as it helps in determining optimum neural architecture (Afolabi et al., 2020b). In this study, 1-20 neurons were investigated for the hidden layer using Levenberg-Marquardt algorithm, the performance for each hidden neuron is shown in Tables 13 and 14. Experimental trials with 14 hidden neurons gave the least MSE and the highest correlation coefficient value. Hence, 14 hidden neuron is considered the most suitable for ANN prediction of CQ adsorption onto HSP1.

In order to determine the transfer function that best predict the experimental data, *logsig, purelin* and *tansig* transfer function were varied, while 14 number of hidden neurons, Levenberg-Marqauardt algorithm were kept constant. Logsig transfer function gave the best prediction for the removal of CQ on HSP1 activated carbon. Fig. 10 presented the architecture of ANN (5-14-1), for the removal of CQ onto HSP1 adsorbent.

Different input variables (HSP1 dosage, CQ initial concentration,

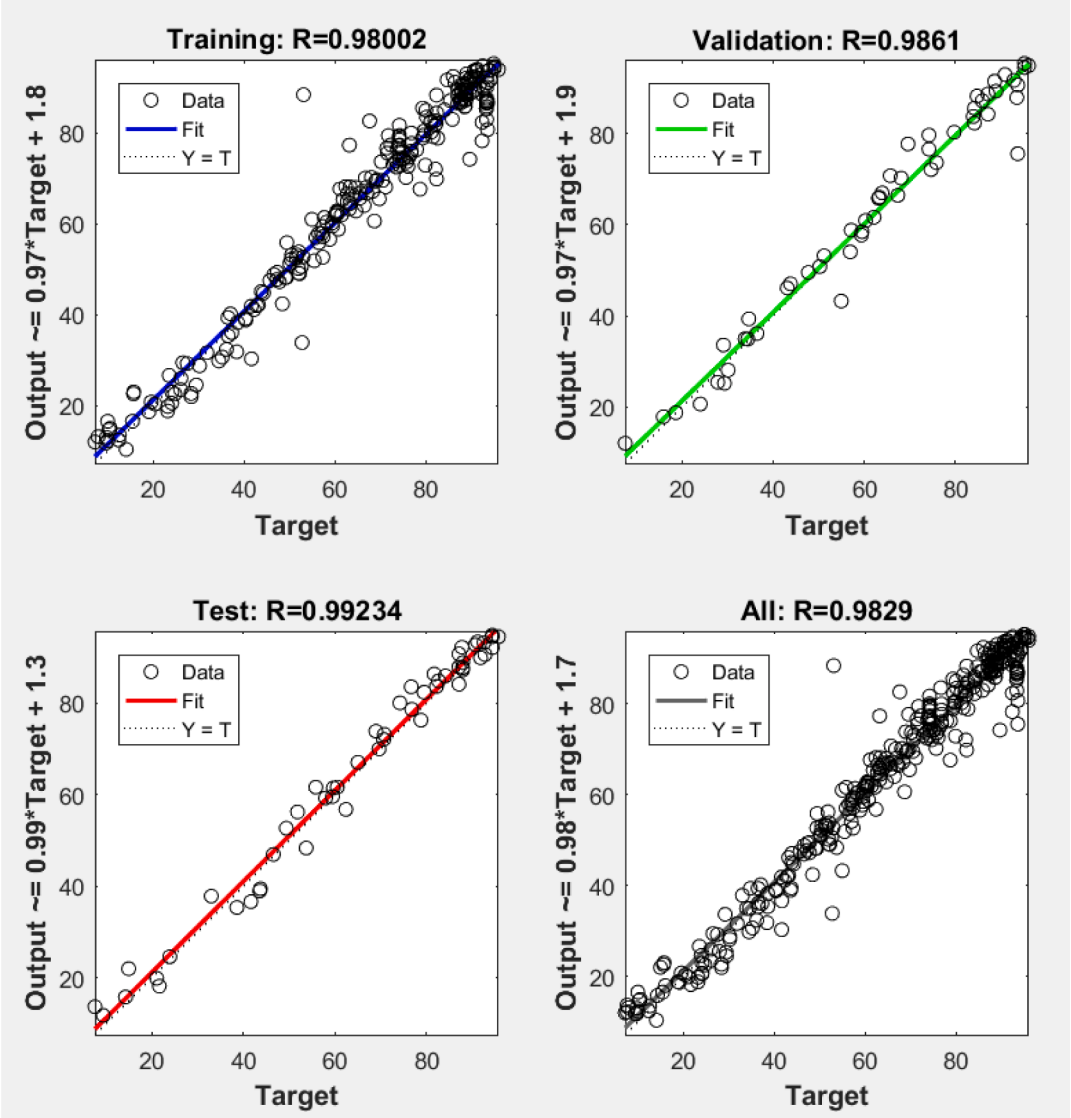

Fig. 9. Comparison of target and predicted values in terms of CQ adsorption efficiency.

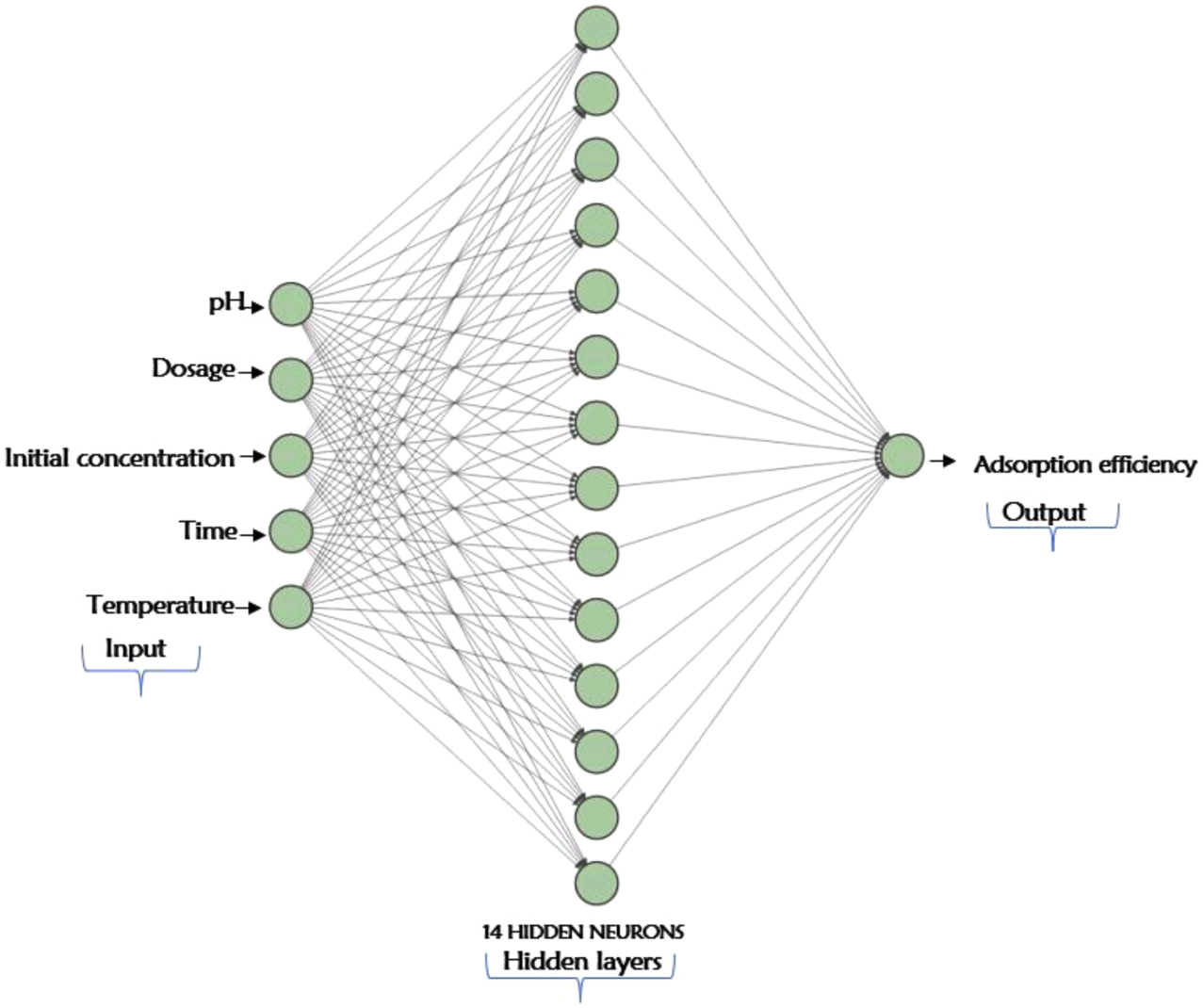

Fig 10. A three-layered ANN architecture for CQ adsorption onto HSP1.

solution pH, temperature and contact time) were used within the trained network. The ANN model that offered the best fit for the training, validation and test, were presented in Fig. 9.

Fig. 11 (a-d) shows the plots of the predicted data obtained during the training using ANN and experimental data at different concentrations and temperatures. The vast agreement between the ANN and the experimental data showed the overview ability of ANN model.

4. Conclusion

HSP1 adsorbent was successfully prepared and used for the adsorption of Chloroquine phosphate from aqueous media. CQ uptake onto HSP1 was found to reliant on pH, contact time, HSP1 dosage, temperature and concentration. The Langmuir monolayer adsorption capacity was obtained to be 161.29 mg/g. The pseudo second order kinetic model provided the best fit. Freundlich adsorption isotherm best fitted the experimental data, indicating a multilayer adsorption process. The thermodynamic studies confirmed the spontaneity, feasibility and the endothermic nature (ΔH^{o} +29.88 KJ mol^{-1}) of the adsorption process. The presence of strong chemical bond between CQ and HSP1 was observed, as the highest percentage desorption recorded was 4.06%, with HCl. The adsorption performance of HSP1 was efficaciously forecasted using Artificial Neural Network (ANN) with 14 hidden neurons. The lowest MSE and the highest correlation coefficient obtained for the ANN models were 8.01 and 0.9872 respectively with precise prediction for adsorption efficiency. A good agreement was recognized between the experimental data and the ANN predicted results. The high capacity displayed by HSP1 for CQ adsorption presents HSP1 as an effective replacement for commercial activated carbon, for the elimination of CQ and perhaps similar environmental pollutants from wastewater.

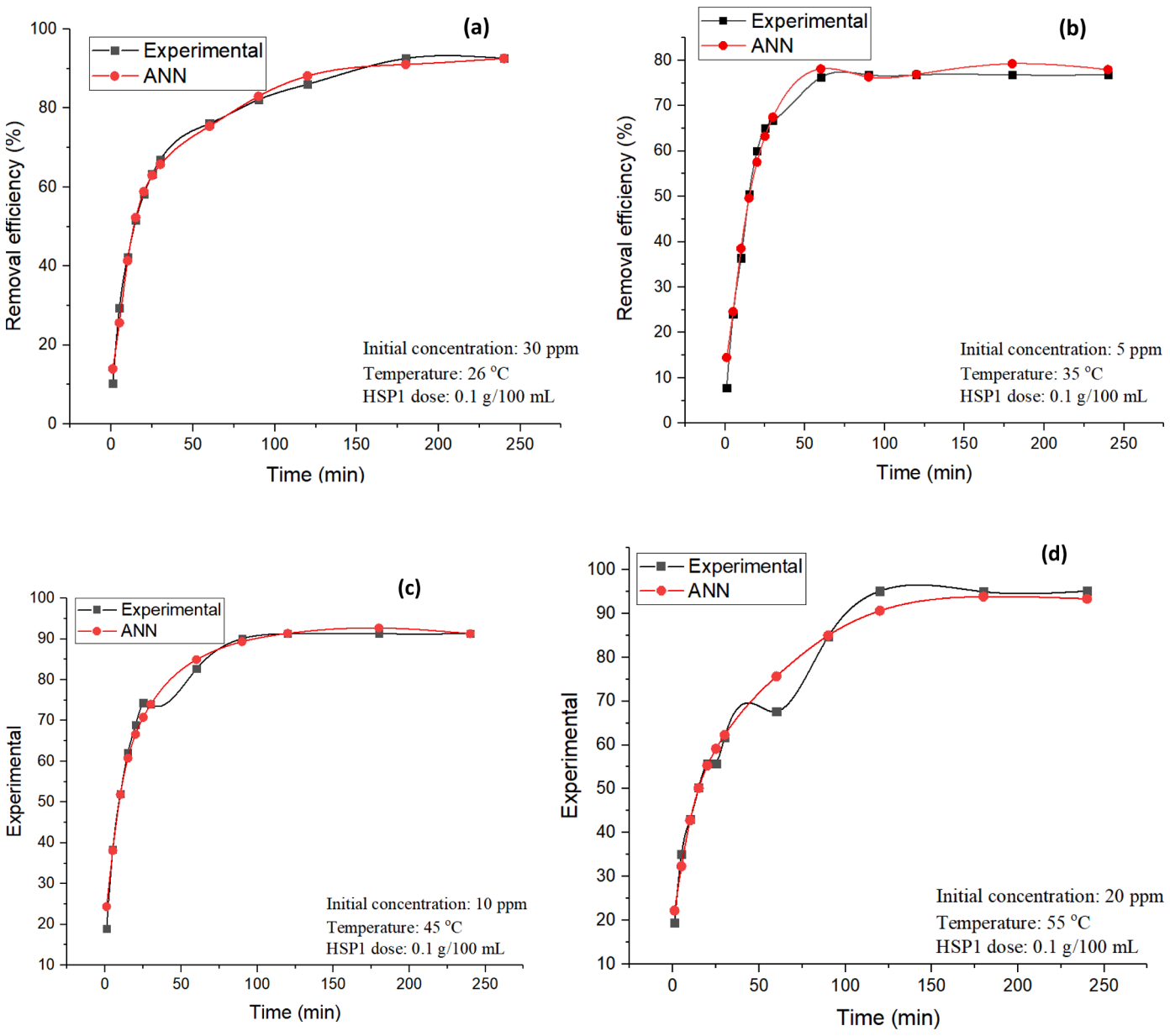

Fig. 11. Plots of adsorption efficiencies at (a) 26 °C (b) 35 °C (c) 45 °C (d) 55 °C.

Declaration of Competing Interest

The authors declare that they have no known competing financial or personal relationship that could appear to have impacted the work reported in this research paper.

References

Abena, P.M., Decloedt, E.H., Bottieau, E., Suleman, F., Adejumo, P., Sam-Agudu, N.A., Muyembe TamFum, J.J., Seydi, M., Eholie, S.P., Mills, E.J., Kallay, O., Zumla, A., Nachega, J.B., 2020. Chloroquine and hydroxychloroquine for the prevention or treatment of COVID-19 in Africa: Caution for inappropriate off-label use in healthcare settings. American Journal of Tropical Medicine and Hygiene 102 (6), 1184–1188. https://doi.org/10.4269/ajtmh.20-0290.

Adewuyi, A., Vargas Pereira, F., 2017. Chemical modifcation of cellulose isolated from underutilized hibiscus sabdariffa via surface grafting: A potential bio-based resource for industrial application. Kemija u Industriji/Journal of Chemists and Chemical Engineers 66 (7–8), 327–338. https://doi.org/10.15255/KUI.2016.024.

Afolabi, I.C., Popoola, S.I., Bello, O.S., 2020a. Machine learning approach for prediction of paracetamol adsorption efficiency on chemically modified orange peel. Spectrochimica Acta - Part A: Molecular and Biomolecular Spectroscopy 243, 118769. https://doi.org/10.1016/j.saa.2020.118769.

Afolabi, I.C., Popoola, S.I., Bello, O.S., 2020b. Modeling pseudo-second-order kinetics of orange peel-paracetamol adsorption process using artificial neural network. Chemometrics and Intelligent Laboratory Systems 203 (January), 104053. https://doi.org/10.1016/j.chemolab.2020.104053.

Aharoni, C., Ungarish, M., 1976. Kinetics of activated chemisorption: Part 1.-The non-elovichian part of the isotherm. Journal of the Chemical Society, Faraday Transactions 1: Physical Chemistry in Condensed Phases 72, 400–408. https://doi.org/10.1039/F19767200400.

Al-Ghouti, M.A., Al-Absi, R.S., 2020. Mechanistic understanding of the adsorption and thermodynamic aspects of cationic methylene blue dye onto cellulosic olive stones biomass from wastewater. Scientific Reports 10 (1), 1–18. https://doi.org/10.1038/s41598-020-72996-3.

Amin, M.T., Alazba, A.A., Shafiq, M., 2015. Adsorptive removal of reactive black 5 from wastewater using bentonite clay: Isotherms, kinetics and thermodynamics. Sustainability (Switzerland) 7 (11), 15302–15318. https://doi.org/10.3390/su71115302.

Auta, M., Hameed, B.H., 2011. Optimized waste tea activated carbon for adsorption of Methylene Blue and Acid Blue 29 dyes using response surface methodology. Chemical Engineering Journal 175 (1), 233–243. https://doi.org/10.1016/j.cej.2011.09.100.

Babić, S., Dabić, D., Ćurković, L., 2017. Fate of hydroxychloroquine in the aquatic environment. In: *15th International Conference on Environmental Science and Technology, September*, pp. 1–5.

Belhachemi, M., Addoun, F., 2011. Comparative adsorption isotherms and modeling of methylene blue onto activated carbons. Applied Water Science 1 (3–4), 111–117. https://doi.org/10.1007/s13201-011-0014-1.

Bello, O.S., Adegoke, K.A., Akinyunni, O.O., 2017. Preparation and characterization of a novel adsorbent from Moringa oleifera leaf. Applied Water Science 7 (3), 1295–1305. https://doi.org/10.1007/s13201-015-0345-4.

Bello, O.S., Alao, O.C., Alagbada, T.C., Agboola, O.S., Omotoba, O.T., Abikoye, O.R., 2021. A renewable, sustainable and low-cost adsorbent for ibuprofen removal. Water Science and Technology 83 (1), 111–122. https://doi.org/10.2166/wst.2020.551.

Bensalah, N., Midassi, S., Ahmad, M.I., Bedoui, A., 2020. Degradation of hydroxychloroquine by electrochemical advanced oxidation processes. Chemical Engineering Journal 402 (April), 126279. https://doi.org/10.1016/j.cej.2020.126279.

da Luz, T.M., Araújo, A.P., da, C., Estrela, F.N., Braz, H.L.B., Jorge, R.J.B., Charlie-Silva, I., Malafaia, G., 2021. Can use of hydroxychloroquine and azithromycin as a treatment of COVID-19 affect aquatic wildlife? A study conducted with neotropical tadpole. Science of the Total Environment 780, 146553. https://doi.org/10.1016/j.scitotenv.2021.146553.

Dada, A.O., Inyinbor, A.A., Bello, O.S., Tokula, B.E., 2021. Novel plantain peel activated carbon–supported zinc oxide nanocomposites (PPAC-ZnO-NC) for adsorption of chloroquine synthetic pharmaceutical used for COVID-19 treatment. Biomass Conversion and Biorefinery. https://doi.org/10.1007/s13399-021-01828-9.

Dehbi, A., Dehmani, Y., Omari, H., Lammini, A., Elazhari, K., Abouarnadasse, S., Abdallaoui, A., 2020. Comparative study of malachite green and phenol adsorption on synthetic hematite iron oxide nanoparticles (α-Fe2O3). Surfaces and Interfaces 21. https://doi.org/10.1016/j.surfin.2020.100637.

Dubinin, M.M., Radushkevich, L.V., 1947. Equation of the characteristic curve of activated charcoal. In: Proceedings of the Academy of Sciences of the USSR: Physical Chemistry Section, 55, pp. 331–337.

Ekpete, O.A., Marcus, A.C., Osi, V., 2017. Preparation and Characterization of Activated Carbon Obtained from Plantain (Musa paradisiaca) Fruit Stem. Journal of Chemistry 2017. https://doi.org/10.1155/2017/8635615.

Fakhri, A., 2017. Adsorption characteristics of graphene oxide as a solid adsorbent for aniline removal from aqueous solutions: Kinetics, thermodynamics and mechanism studies. Journal of Saudi Chemical Society 21 (October 2013), S52–S57. https://doi.org/10.1016/j.jscs.2013.10.002.

Fernandez, M.E., Nunell, G.V., Bonelli, P.R., Cukierman, A.L., 2010. Effectiveness of Cupressus sempervirens cones as biosorbent for the removal of basic dyes from aqueous solutions in batch and dynamic modes. Bioresource Technology 101 (24), 9500–9507. https://doi.org/10.1016/j.biortech.2010.07.102.

Freundlich, H.M., 1906. Over theadsorption in solution. Z. Phys. Chem. 57, 385–470.

Hamdaoui, O., Naffrechoux, E., 2007. Modeling of adsorption isotherms of phenol and chlorophenols onto granular activated carbon. Part I. Two-parameter models and equations allowing determination of thermodynamic parameters. Journal of Hazardous Materials 147 (1–2), 381–394. https://doi.org/10.1016/j.jhazmat.2007.01.021.

Ho, Y.S., McKay, G., 1998. Sorption of dye from aqueous solution by peat. Chemical Engineering Journal 70 (2), 115–124. https://doi.org/10.1016/S1385-8947(98)00076-X.

INYINBOR, A.A., Adekola, F.A., Bello, O.S., Bankole, D.T., Oreofe, T.A., Lukman, A.F., Olatunji, G.A., 2022a. Surface functionalized plant residue in cu2+ scavenging: Chemometrics of operational parameters for process economy validation. South African Journal of Chemical Engineering 40 (February), 144–153. https://doi.org/10.1016/j.sajce.2022.03.001.

Inyinbor, A.A., Adekola, F.A., Olatunji, G.A., 2015. Adsorption of rhodamine b dye from aqueous solution on Irvingia gabonensis biomass: Kinetics and thermodynamics studies. South African Journal of Chemistry 68 (1), 115–125. https://doi.org/10.17159/0379-4350/2015/v68a17.

Inyinbor, A.A., Adekola, F.A., Olatunji, G.A., 2019. Low cost adsorbent prepared from Vigna subterranean waste: Physicochemical, morphological and surface chemistry data set. Chemical Data Collections 24. https://doi.org/10.1016/j.cdc.2019.100294.

IWUAGWU, M.A., ALOKO, K.S., 1992. Adsorption of Paracetamol and Chloroquine Phosphate by Some Antacids. Journal of Pharmacy and Pharmacology 44 (8), 655–658. https://doi.org/10.1111/j.2042-7158.1992.tb05488.x.

Kårelid, V., Larsson, G., Björlenius, B., 2017. Pilot-scale removal of pharmaceuticals in municipal wastewater: Comparison of granular and powdered activated carbon treatment at three wastewater treatment plants. Journal of Environmental Management 193, 491–502. https://doi.org/10.1016/j.jenvman.2017.02.042.

kaur, K., Rani, S., Mahajan, K., 2012. Congo Red Biowaste Materials as Adsorbents. Journal of Chemistry 2013, 12.

Kavitha, B., Sarala Thambavani, D., 2020. Artificial neural network optimization of adsorption parameters for Cr(VI), Ni(II) and Cu(II) ions removal from aqueous solutions by riverbed sand. Iranian Journal of Chemistry and Chemical Engineering 39 (5), 203–223. https://doi.org/10.30492/ijcce.2020.39785.

Khalili, H., Ebrahimian Pirbazari, A., Saraei, F.E.K., Mousavi, S.H., 2021. Simultaneous removal of basic dyes from binary systems by modified orange peel and modeling the process by an intelligent tool. Desalination and Water Treatment 221 (June), 406–427. https://doi.org/10.5004/dwt.2021.27039.

Khan, T., Mustafa, M.R.U., Isa, M.H., Manan, T.S.B.A., Ho, Y.C., Lim, J.W., Yusof, N.Z., 2017. Artificial Neural Network (ANN) for Modelling Adsorption of Lead (Pb (II)) from Aqueous Solution. Water, Air, and Soil Pollution (11), 228. https://doi.org/10.1007/s11270-017-3613-0.

Lagergren, S., 1898. On the theory of so-called adsorption of dissolved substances. Kungliga Svenska Vetenskapsakademiens Handlingar 24 (4), 1–39.

Langmuir, I., 1917. The constitution and fundamental properties of solids and liquids. Journal of the Franklin Institute 183 (1), 102–105. https://doi.org/10.1016/S0016-0032(17)90938-X.

Lei, Z.N., Wu, Z.X., Dong, S., Yang, D.H., Zhang, L., Ke, Z., Zou, C., Chen, Z.S., 2020. Chloroquine and hydroxychloroquine in the treatment of malaria and repurposing in treating COVID-19. Pharmacology and Therapeutics 216, 107672. https://doi.org/10.1016/j.pharmthera.2020.107672.

Lindroos, M., Hörnström, D., Larsson, G., Gustavsson, M., van Maris, A.J.A., 2019. Continuous removal of the model pharmaceutical chloroquine from water using melanin-covered Escherichia coli in a membrane bioreactor. Journal of Hazardous Materials 365 (October 2018), 74–80. https://doi.org/10.1016/j.jhazmat.2018.10.081.

Lopes, E.C.N., Dos Anjos, F.S.C., Vieira, E.F.S., Cestari, A.R., 2003. An alternative Avrami equation to evaluate kinetic parameters of the interaction of Hg(II) with thin chitosan membranes. Journal of Colloid and Interface Science 263 (2), 542–547. https://doi.org/10.1016/S0021-9797(03)00326-6.

M, T., G, B, 2020. Various Absorbents and Parameters Affecting Removal of Water Hardness from Wastewater: Review. International Journal of Water and Wastewater Treatment 6 (3), 1–20. https://doi.org/10.16966/2381-5299.173.

Margot, J., Rossi, L., Barry, D.A., Holliger, C., 2015. A review of the fate of micropollutants in wastewater treatment plants. WIREs Water 2 (5), 457–487. https://doi.org/10.1002/wat2.1090.

Obayomi, K.S., Oluwadiya, A.E., Lau, S.Y., Dada, A.O., Akubuo-Casmir, D., Adelani-Akande, T.A., Fazle Bari, A.S.M., Temidayo, S.O., Rahman, M.M, 2021. Biosynthesis of Tithonia diversifolia leaf mediated Zinc Oxide Nanoparticles loaded with flamboyant pods (Delonix regia) for the treatment of Methylene Blue Wastewater. Arabian Journal of Chemistry 14 (10), 103363. https://doi.org/10.1016/j.arabjc.2021.103363.

Ojediran, J.O., Dada, A.O., Aniyi, S.O., David, R.O., Adewumi, A.D., 2021. Mechanism and isotherm modeling of effective adsorption of malachite green as endocrine disruptive dye using Acid Functionalized Maize Cob (AFMC). Scientific Reports 11 (1), 1–15. https://doi.org/10.1038/s41598-021-00993-1.

Pauletto, P.S., Lütke, S.F., Dotto, G.L., Salau, N.P.G., 2021a. Adsorption mechanisms of single and simultaneous removal of pharmaceutical compounds onto activated carbon: Isotherm and thermodynamic modeling. Journal of Molecular Liquids 336, 116203. https://doi.org/10.1016/j.molliq.2021.116203.

Pauletto, P.S., Lütke, S.F., Dotto, G.L., Salau, N.P.G., 2021b. Forecasting the multicomponent adsorption of nimesulide and paracetamol through artificial neural network. Chemical Engineering Journal 412 (October 2020), 127527. https://doi.org/10.1016/j.cej.2020.127527.

Prasad, A.L., Santhi, T., Manonmani, S., 2015. Recent developments in preparation of activated carbons by microwave: Study of residual errors. Arabian Journal of Chemistry 8 (3), 343–354. https://doi.org/10.1016/j.arabjc.2011.01.020.

Ringot, D., Lerzy, B., Chaplain, K., Bonhoure, J.P., Auclair, E., Larondelle, Y., 2007. In vitro biosorption of ochratoxin A on the yeast industry by-products: Comparison of isotherm models. Bioresource Technology 98 (9), 1812–1821. https://doi.org/10.1016/j.biortech.2006.06.015.

Schroeder, R.L., Gerber, J.P., 2014. Chloroquine and hydroxychloroquine binding to melanin: Some possible consequences for pathologies. Toxicology Reports 1, 963–968. https://doi.org/10.1016/j.toxrep.2014.10.019.

Schroeder, R.L., Pendleton, P., Gerber, J.P., 2015. Physical factors affecting chloroquine binding to melanin. Colloids and Surfaces B: Biointerfaces 134, 8–16. https://doi.org/10.1016/j.colsurfb.2015.06.040.

Shuaihua, L., Qionghua, Z., Yixin, O., Yilv, G., Qiang, L., Jinlan, W., 2018. Accelerated discovery of stable lead-free hybrid organic-inorganic perovskites via machine learning. Nature Communications 9 (1), 3405.

Singh, P., Dobhal, R., Singh, R., Gupta, S., Rana, R.S., Kandari, V., 2014. A review on characterization and bioremediation of pharmaceutical industries' wastewater: an Indian perspective. Applied Water Science 7 (1), 1–12.

Tarawou, T., Young, E., 2015. Intraparticle and Liquid film Diffusion Studies on the Adsorption of Cu 2+ and Pb 2+ Ions from Aqueous Solution using Powdered Cocoa Pod (Theobroma cacao). International Research Journal of Engineering and Technology 2356–2395. https://www.irjet.net/archives/V2/i8/IRJET-V2I841.pdf.

Thommes, M., Kaneko, K., Neimark, A.V., Olivier, J.P., Rodriguez-Reinoso, F., Rouquerol, J., Sing, K.S.W., 2015. Physisorption of gases, with special reference to the evaluation of surface area and pore size distribution (IUPAC Technical Report). Pure and Applied Chemistry 87 (9-10), 1051–1069. https://doi.org/10.1515/pac-2014-1117.

Wang, Z., Zhang, H., Ren, J., Lin, X., Han, T., Liu, J., Li, J., 2021. Predicting adsorption ability of adsorbents at arbitrary sites for pollutants using deep transfer learning. Npj Computational Materials 7 (1), 1–9. https://doi.org/10.1038/s41524-021-00494-9.

Weber, W.J., Morris, J.C., 1963. Closure to "Kinetics of Adsorption on Carbon from Solution. Journal of the Sanitary Engineering Division 89 (6), 53–55. https://doi.org/10.1061/jsedai.0000467.

Xue, Y., Du, C., Wu, Z., Zhang, L., 2018. Relationship of cellulose and lignin contents in biomass to the structure and RB-19 adsorption behavior of activated carbon. New Journal of Chemistry 42 (20), 16493–16502. https://doi.org/10.1039/c8nj03007c.

Yuan, R., Liu, Z., Balachandran, P.V., Xue, D., Zhou, Y., Ding, X., Sun, J., Xue, D., Lookman, T., 2018. Accelerated Discovery of Large Electrostrains in BaTiO3-Based Piezoelectrics Using Active Learning. Advanced Materials (7), 30. https://doi.org/10.1002/adma.201702884.